



**HAL**  
open science

## Computational approach and electrochemical measurements for protein detection with MIP-based sensor

Zouhour Mazouz, Meriem Mokni, Najla Fourati, Chouki Zerrouki, Florent Barbault, Mahamadou Seydou, Rafik Kalfat, Nourdin Yaakoubi, Asma Omezzine, Ali Bouslema, et al.

► **To cite this version:**

Zouhour Mazouz, Meriem Mokni, Najla Fourati, Chouki Zerrouki, Florent Barbault, et al.. Computational approach and electrochemical measurements for protein detection with MIP-based sensor. *Biosensors and Bioelectronics*, 2020, 151, pp.111978. 10.1016/j.bios.2019.111978 . hal-02464043

**HAL Id: hal-02464043**

**<https://univ-lemans.hal.science/hal-02464043>**

Submitted on 21 Jul 2022

**HAL** is a multi-disciplinary open access archive for the deposit and dissemination of scientific research documents, whether they are published or not. The documents may come from teaching and research institutions in France or abroad, or from public or private research centers.

L'archive ouverte pluridisciplinaire **HAL**, est destinée au dépôt et à la diffusion de documents scientifiques de niveau recherche, publiés ou non, émanant des établissements d'enseignement et de recherche français ou étrangers, des laboratoires publics ou privés.



Distributed under a Creative Commons Attribution - NonCommercial 4.0 International License

## Computational approach and electrochemical measurements for protein detection with MIP-based sensor

Zouhour Mazouz<sup>a,b</sup>, Meriem Mokni<sup>c,d</sup>, Najla Fourati<sup>c,\*</sup>, Chouki Zerrouki<sup>c</sup>,  
Florent Barbault<sup>e</sup>, Mahamadou Seydou<sup>e</sup>, Rafik Kalfat<sup>a</sup>, Nourdin Yaakoubi<sup>f</sup>,  
Asma Omezzine<sup>d</sup>, Ali Bouslema<sup>d</sup>, Ali Othmane<sup>b</sup>

- a. INRAP, Laboratoire Méthodes et Techniques d'Analyse, BiotechPole, 2020, Sidi-Thabet, Tunisia.
- b. Université de Monastir, Faculté de Médecine de Monastir, LIMA, Av. Avicenne, 5019, Monastir, Tunisia
- c. Cnam, SATIE, UMR CNRS 8029, 292 rue Saint Martin, 75003, Paris, France.
- d. Hôpital Universitaire Sahloul, Service de Biochimie, 4011, Sousse, Tunisia.
- e. Université de Paris, ITODYS, CNRS, UMR 7086, 15 rue J-A de Baïf, F-75013 Paris, France.
- f. Le Mans Université, LAUM, UMR CNRS 6613, Avenue Olivier Messiaen, 72085 Le Mans, France.

\* Corresponding author. Email: [fourati@cnam.fr](mailto:fourati@cnam.fr); tel :+(33)158808703

### Abstract

Rapid and accurate detection of proteins in biological fluids is increasingly required in the biomedical environment. Actually, it is performed with conventional techniques, which are generally run by robotized platforms at centralized laboratories. In this work, molecular dynamics calculations and an experimental procedure were conducted to set up electrochemical sensors based on polypyrrol (PPy) molecular imprinted polymers (MIP) for proteins detection. Here, prostate-specific antigen (PSA) was selected as a template model. Computational calculations indicate that for any PPy conformation and any amino-acid location in the protein, PSA molecules remain strongly inserted in the PPy polymer without biological alterations. One from possible orientations, appeared to be most probable as it presents the lowest absorption energy ( $-363 \text{ kcal.mol}^{-1}$ ) and largest contact area ( $4034.1 \text{ \AA}^2$ ). The device was then elaborated by in situ electropolymerization of PPy films. MIP's thickness and extraction duration were optimized by chronoamperometry. Square wave voltammetry technique was investigated for PSA detection in standard solution in the concentration range of  $3 \times 10^{-8} \text{ ng.ml}^{-1}$ -  $300 \text{ ng.ml}^{-1}$ . According to the Hill equation, the equilibrium dissociation constant

$K_d$  between PSA and its imprint was estimated at  $K_d = (1.02 \pm 0.54) \times 10^{-14}$  M, confirming the strong binding between the designed MIP and the protein as predicted by the computational study. PSA concentration values directly measured in 35 human serum samples were found closely correlated to those measured by the ELISA technique. The promising fast and low-cost sensor might be used successfully for proteins detection at low concentrations with high selectivity and reproducibility.

**Key words:** Molecularly imprinted polymer (MIP); Molecular Dynamic computations; electrochemical biosensor; protein detection

## 1. Introduction

Accurate and selective detection of proteins in complex biological fluids is an important issue in clinical diagnostics, biomedical applications and proteomics research (De et al., 2009; Wilson., 2009). Protein biomarkers particularly indicate a normal or pathogenic biological process. Currently, they are detected by conventional techniques such as high-performance liquid chromatography-mass spectrometric (HPLC-MASS) (Ogasawara., et al., 2015), enzyme-linked immunosorbent assays (ELISA) (Vasilescu et al., 2013), fluorescence immunoassay or bioluminescent immunoassay (Akter et al., 2015). However, and despite their accuracy and high sensitivity, these techniques require expensive instruments and need complex separation and treatment steps. In view of these limitations and of the greatest interest of proteins detection, the development of biosensors technology is likely to emerge as a significant challenge in this analytical field. Electrochemical biosensors have been specially investigated due to their low cost, fast response, sensitivity, and the further possibility of their automation and miniaturization. Nevertheless, these devices also present some limitations concerning the nature of bioactive sensing layer and its immobilization process. For example, specific antibodies are generally expensive and not indefinitely stable at room temperature. The polyclonal ones may differ from an animal to another one, while monoclonal antibodies

may be sensitive to subtle changes in the epitope. Concerning the immobilization methods on transducers surfaces, which have a key-role in the performance of biosensors, various strategies have been considered to successfully immobilize the bioreceptor. However, depending on the considered functionalization approach, the reproducibility of the interaction between the bioreceptor and the target protein could be significantly affected leading to a quasi-impossible sensors' regeneration. Researches have therefore been oriented to the development of synthetic receptors able to mimic the natural and selective interaction between two biological entities such as Ac/Ag or enzyme/substrate: the molecular imprinted polymers (MIPs).

By operating through a lock - key mechanism, MIPs can selectively bind the analytes of interest with which they were templated during the polymerization process (Bel Bruno., 2019). Molecular imprinting can be achieved via either covalent, semi-covalent or non-covalent binding between functional monomers and imprint molecules. Together, they interact to form a complex during the polymerization process. The templates are after that removed from the vicinity of the polymeric matrix leaving cavities available for the selective rebinding of the analytes of interest. Compared to biological entities, MIPs have numerous advantages: chemical and physical stability, ease of preparation, possibility of long period-storage without freezing, and regeneration.

To achieve the best MIP design, bulk imprinting approach was investigated for small molecules detection, while electropolymerization was found more appropriate for large molecules, such as virus, cells and proteins. The electropolymerization method appeared thus as a promising alternative to modify a conventional electrode as it allows macro-biomolecules diffusion in a polymeric matrix and facilitates templates removal and rebinding (Frasco et al., 2017; Dabrowski et al., 2018; El-Sharif et al., 2017). It also offers other advantages mainly an easy adherence of the polymeric films to the surface of conducting

electrodes, of any shape and size, and the ability to control thickness of the films under different depositions conditions (Dabrowski et al., 2017).

MIPs based sensors were investigated in the sensing of different chemical and biological molecules including illegal drugs and additives (Xiao et al., 2018), pesticides (Farooq et al., 2018; Mazouz et al., 2017), antibiotics (Mohsenzadeh et al., 2018; Ktari et al., 2015), ions (Fu et al., 2015), amino acids (Scorrano et al., 2011), nucleotides ( Spivak and Shea, 1998), neurotransmitters (Si and Song, 2018) and as delivery systems of anticancer agents (CA et al., 2018).

For proteins detection, the technology of molecular imprinting is certainly robust and accurate but remains highly dependent on functional monomers nature. Different molecules, o-phenylenediamine (Zhao et al., 2017), dopamine (Lai et al., 2018), aniline (Rao et al., 2017), thiophene (Dabrowski et al., 2017), and pyrrole (Zeng et al., 2017), have been already tested for the detection of several kinds of proteins, like insulin, carcinoma embryonic antigen, creatinine, and ovalbumin.

A specific protein called prostate-specific antigen (PSA) has often been selected and detected using classic biosensors (Hwang et al., 2017; Khan et al., 2018; Zhang et al., 2018). However, only few works have reported the design of MIP based electrochemical sensors for PSA detection. Despite their good metrological performances, the proposed strategies are often complicated, as they need the further use of nanomaterials, such as nanoparticles and carbon nanotubes (Patra et al., 2015) or graphene nanoplates (Ma et al., 2017) to enhance the sensitivity of the designed biosensors. In addition, the involved processes are generally time and reagents consuming (Rebelo et al., 2014; Ertürk et al., 2015; Jolly et al., 2016; Yazdani et al., 2018), making difficult the transfer of the know-how to industrial fields in general, and the pharmaceutical one, in particular.

To overcome these drawbacks and to achieve successful design of a given MIP, a careful understanding of the interaction between functional monomers and the protein template is needed. Besides, determining, among possible spatial configurations, the most probable one will permit to predict the stability of the MIP/template complex according to the number of involved interactions, and thus the effectiveness of exclusive, or at least selective, recognition. Computational studies were often addressed to interactions between biopolymers and solid surfaces (Ruan et al., 2017). Only few investigations have been performed on MIP/biomolecule descriptions. To date, two main strategies have been explored: i) the analyte was a small molecule and thus direct investigations with one or few surrounded monomers were performed and decipher a cavity (Chianella et al., 2006; Rodríguez-Dorado et al., 2016) which could be analyzed as molecular interaction fields (Monti et al., 2006); ii) a macro-molecule, such as protein, was considered. In this case, only few monomers were either docked on the protein surface (Borožnjak et al., 2017) or manually placed and further optimized (Chianella et al., 2002). But, as far as we know, no direct simulation of a large analyte associated with a large mimicked polymer, respecting its experimental density, has been investigated.

Here, polypyrrole (PPy) was chosen among the large variety of conducting polymers as it can be used in a neutral pH region, is stable and can conveniently be electropolymerized on various substrate materials. PPy has already been investigated as a polymeric matrix of molecular imprinted polymers designed for the detection of both low molecular weight analytes, such as paracetamol (Ozcan and Sahin, 2007), caffeine (Ebarvia et al., 2005), ascorbic acid (Özcan et al., 2008), and those having high molecular weight such as glycoproteins and enzymes (Ramanaviciene and Ramanavicius, 2004). Nevertheless, several difficulties might be encountered during the imprinting process of proteins, mainly: i) possibility of protein denaturation during polymerization ii) the large size of the proteins

makes them difficult to remove from the vicinity of the polymeric matrix or to rebind to a highly cross-linked polymeric network; and iii) insufficient number of interactions between protein amino-acids and the PPy residues, leading to an unstable complex (Dabrowski et al., 2018).

Templates removal is another critical parameter which conditions the capacity of a given MIP to recognize the analytes of interest. Several pitfalls must in fact been avoided such as incomplete removal of the proteins, cavities rupture during washing steps, collapse of the cavities after templates removal and distortion of the monomers/proteins binding points. In order to remove the entrapped template, different strategies are possible. They are generally based on one or a combination of the following approaches: a) the use of solvents that strongly interact with the polymer and may lead to the required swelling of the back-bone necessary for template release (Erdossy et al., 2016; El-Sharif et al., 2017), b) the use of acid or basic solvents in order to disrupt the electrostatic interactions between protein and polymer (Lorenzo et al., 2011) c) the super-imposition of a constant ac voltage onto a constant potential (0.50 V vs. Ag/AgCl) (Sindhu et al., 2016) and d) and physically-assisted extraction (via ultrasound, microwave or pressurized liquid extractions) (El-Sharif et al., 2017 ).

The aim of this work is to highlight the contribution of the computational studies in the elaboration of a PPy molecular imprinted polymer for sensitive detection of prostate specific antigen (PSA, MW = 32 kDa), a template model chosen for its clinical interest.

The computational investigations produced here were quite complex but are however original and should provide a referring work, as it could be extended to various diagnostically relevant proteins using not only aptamers but also other affinity molecules such as peptides, affirmers and antibody fragments.

After in situ electropolymerization of PPy films on gold electrode surfaces, PSA templates were removed from the vicinity of the polymeric matrix by a sur-saturated sodium chloride

solution, an eco-friendly solvent. Square wave voltammetry was then investigated to follow up the response of the MIP-based sensor towards PSA analytes detection and to perform selectivity tests.

To evaluate the accuracy of the designed PPy-PSA-MIP sensor, PSA concentration quantifications were conducted in real human serum samples extracted from 35 patients. Results were then compared to those obtained by the enzyme-linked immunosorbent assay (ELISA), considered as the golden standard technique in the hospital environment.

## **2. Materials and methods**

### **2.1. Reagents**

Sulfuric acid ( $\text{H}_2\text{SO}_4$ , 95%), acetic acid ( $\text{CH}_3\text{COOH}$ ), hydrogen peroxide ( $\text{H}_2\text{O}_2$ , 30%), methanol ( $\text{CH}_3\text{OH}$ ), lithium perchlorate ( $\text{LiClO}_4$ ) and phosphate buffer saline (PBS) were purchased from sigma Aldrich and used as received. Pyrrole (Py) was purified before use by filtering through basic alumina column and stored in dark at  $4^\circ\text{C}$ . PSA protein was purchased from Bio-Rad Laboratories.

### **2.2. Electrochemical measurements**

Chronamperometry (CA) and square wave voltammetry (SWV) were performed with a CHI 660C workstation (CHI instruments, Inc IJ Cambria Scientific Ltd., Llwynhendy, UK) with a three-electrode configuration: a gold electrode, a saturated calomel electrode (SCE), and a platinum wire, as the working, the reference and the auxiliary electrodes, respectively. All experiments were carried out at room temperature and under ambient air.

### **2.3. Atomic force microscopy (AFM)**

AFM measurements were carried out with a Nanosurf easyScan 2 Flex system in the phase contrast mode. The used cantilevers were SSS-NCLR type (Super Sharp Silicon probes from Nanosensors, Switzerland) with a resonance frequency of about 190 kHz. The AFM probe's

curvature radius was inferior to 2 nm and the half cone angle was inferior to 10° at 200 nm from apex.

#### **2.4. Fourier transform infrared spectroscopy (FTIR)**

FTIR analyses were carried out with a Perkin Elmer “spectrum two” spectrometer equipped with an attenuated total reflectance (ATR) cell. The spectra were recorded at room temperature in the range 500 – 4000  $\text{cm}^{-1}$  with a resolution of 2  $\text{cm}^{-1}$ . A background spectrum was recorded prior to each sample measurement and was used for background correction.

#### **2.5. Computational study**

3D coordinates of the PSA protein were extracted from the protein data bank [WEB1] and correspond to the Xray structure of human PSA (Stura et al., 2011). Hydrogen atoms along with the specification of disulphide bridges were generated with the leap module of Amber 16 (Case et al., 2018) through the ff14SB protein force-field (Maier et al., 2015) definition. To create MIP of PSA, a volume of  $7.5 \times 8.1 \times 7.4 = 449.55 \text{ nm}^3$  was created around the PSA protein. This volume was chosen so that any atom of the protein is extended to, at least, a distance of 15 Å. The generated box was then filled by 2509 polypyrrole (PPy) molecules with the software packmol (Martínez et al., 2009) in order to reach the PPy desired density of  $1.5 \text{ g/cm}^3$ . Both the *cis* and *trans* configurations, named PPyt and PPyc respectively, were considered in the ratio obtained according to Boltzmann distribution applied to their free enthalpies ( $\Delta G$ ) which are determined by quantum chemical calculations at MP2/6-311+G\*\*. The *trans* conformation is found more stable than *cis* one by 1.44 kcal/mol. This corresponds to 2283 PPyt and 226 PPyc molecules used in the box.

At this point, the PSA is completely covered by PPy molecules so that it is impossible for the protein to escape and thus the MIP is not functional. Therefore, to mimic an active PSA MIP, the system was cut according to the X, Y and Z directions, as shown on Fig.S1, so that the intersection of the three plans is located on the center of mass of the PSA. For each plan, two

orientations are kept and arbitrarily named "top" or "down" as displayed on Fig.S1 This way, 6 starting orientations were obtained and used as starting points for MD computations.

Prior to launch MD, the 6 systems were immersed in TIP3P water rectangular boxes by extending each system on the direction not covered by the MIP by a distance of 20 Å from any atoms. The number of water molecules for each systems is around 13 000 and two chlorine anion were added to neutralize the +2 global charge of PSA in order to use Particle-Mesh Ewald technique (Darden et al., 1993) to treat the electrostatic potential during the MD computations under periodic boundary conditions.

The simulation protocol started with 10000 minimizations steps in order to remove any potential vacuum bubbles. During this stage, the PPy and PSA molecules were kept frozen to their initial positions with harmonic restraints of 100 kcal/mol.Å<sup>2</sup>. These restraints were then removed, and systems were minimized with 20000 steps in order to get structures with low potential energy.

In order to mimic the behavior of a polymer, the PPy carbon atom at the junction between the pyrrole rings were constrained with harmonic restraints of 5 kcal/mol.Å<sup>2</sup> during all the steps of the MD computations, for the 6 systems. This way, the density of MIP remains roughly constant during the simulations while the PPyt and PPyC residues can rotate to accommodate their positions toward PSA. The SHAKE algorithm (Ryckaert et al., 1977) was used for all covalent bonds containing a hydrogen atom allowing to use a time increment of 2 fs. The MD protocol started with a heating phase of 1 ns where temperature is gradually increased from 0 to 300 K. After these heating phases, all systems were switched on NTP conditions for 1 ns in order to equilibrate their solvents. Finally, 6 MD productions in the NVT ensemble were produced for 100 ns each.

Visual Molecular Dynamics (VMD) software (Humphrey et al., 1996) was employed to visualize the MD trajectories of systems and make the figures. Root mean square deviations

(RMSD) and other structural analyses were computed with the cpptraj module (Roe and Cheatham, 2013) of Amber. The 6 representative structures of the systems were extracted from their trajectories by selecting the conformation which displayed the lowest RMSD of their average coordinates. The interaction energies between MIP and PSA were computed according to a previously published protocol (Touzeau et al., 2018). In summary, 1000 snapshots were extracted from the last 50 ns of the 6 equilibrated trajectories (every 50 ps) and correspond to the adsorbed states of each system. The 6 desorbed states were artificially created by moving away the PSA from the polymer by a distance of 50 Å. After 1000 steps of minimization, the adsorption energies were computed by averaging the energies differences between the adsorbed and desorbed states.

To decipher the interactions between PSA amino-acids and the PPy residues of MIP, several characteristics have been defined. First, the interactions were identified as "border" (B) or "deep" (D) according to the plan delimiting the interface between water and MIP. If the amino-acid crosses this plan, its interaction were defined as border (i.e near the solvent) while the interaction is more deeply located inside the MIP. This distinction is made according to our knowledge on protein ligand interaction (Heredia et al., 2015; Jonquoy et al., 2011) for which, generally, the border interactions are useful to orient the ligand inside the protein cavity whereas the deepest interactions reinforce the stability of the complex. The second distinction concerns the atoms involved in the protein/PPy interaction. If the protein atoms belong to the peptidic moieties, the interaction is marked as "backbone" (b) otherwise the interaction is marked as "sidechain" (s). This distinction was investigated since backbone atoms are identical for all amino-acids of a protein and might not be perturbed if the residue is mutated. Finally, the last structural identification recorded is the conformation of PPy which can be either *cis* (PPyc) or *trans* (PPyt).

## 2.6. Electrosynthesis of polypyrrole imprinted and non-imprinted polymers

Prior to MIP electrosynthesis, gold electrodes surfaces were cleaned and activated with a piranha solution ( $\text{H}_2\text{SO}_4$  98% /  $\text{H}_2\text{O}_2$  30%, 1:1 v/v) during 2 min. The substrates were then copiously rinsed with deionized double distilled (DI) water, then with ethanol before being dried under ambient air.

A thin PPy blocking layer (BL) was then electrodeposited on gold substrates by chronoamperometry (CA) at a constant potential of 1.05 V vs. SCE. Here after the different parameters corresponding to the CA experiment: low  $E(\text{V}) = 0$ , step = 1, pulse width = 2 s, Quiet time = 5 s and sensitivity ( $A/V$ ) =  $1e-003$ . The BL permits in fact to prevent the formation of PSA/gold complexes and to reduce the oxidation potential of pyrrole during the preparation of the MIP.

PSA-PPy imprinted polymers were then prepared by CA at a fixed potential of 1.05 V vs. SCE with the following concentrations:  $[\text{PPy}] = 10^{-2}$  M,  $[\text{PSA}] = 3.10^{-8}$  M and  $[\text{LiClO}_4] = 10^{-1}$  M. The pH of the prepolymerization solution was equal to 7.4.

The corresponding non-molecularly imprinted polymer, NIP, was prepared with the same procedures in the absence of PSA templates.

## 3. Results and discussion

### 3.1. Computational results

For all MD simulations, the kinetic, potential, and overall energies were monitored along the trajectory, as well as the densities, pressures or volumes, and temperatures. All these data demonstrate the consistency of the studied systems. To evaluate the movement made by the PSA protein along the molecular trajectory we computed root mean square deviation (RMSD). The 6 RMSD curves representing the 100 ns molecular dynamics trajectories of all directions are presented in supplementary materials (Fig. S2). For all orientations, the recorded deviations of PSA from its crystal structure are very low and never exceed 2.0 Å for the backbone atoms and 3.2 Å when all atoms are considered. These values must be

compared to what can be observed experimentally since an older crystal structure of PSA have been determined by the same team (Ménez et al., 2008) and the difference between these two experimental structures are of 2.8 Å for the backbone atoms and 3.5 Å for all atoms. Therefore, our results strongly demonstrate that the MIP environments of PPy do not induce major modification of the PSA protein which thus remains biologically active.

At the end of the 100 ns of molecular dynamics simulations, all PSA molecules remain inserted in the PPy polymer whatever are the starting orientations. This emphasizes the adaptable behaviour of PPy polymer toward a solute and illustrates why this polymer is usually chosen to create MIPs. However, it is of high interest to enquiry if all orientations are equally probable. Adsorption energies were thus computed.

Results gathered in table 1 indicate that the adsorption energies are negative for all orientations, which attests the feasibility of the device and thermodynamically validate our strategy to use polypyrrole as a polymeric matrix. Moreover, the energy values were ranged from -270.4 to -363.3 kcal/mol for PYD and PXD orientations respectively.

**Table. 1.** Adsorption energies of PSA onto MIP for the six studied orientations. The "contact surface" column represents, for each system, the protein surface inserted in the PPy polymer whereas the %Prot is the percentage of protein surface in contact with the MIP.

<b>Orientation</b>	<b><math>\Delta E</math> (kcal/mol)</b>	<b>Contact surface Å<sup>2</sup></b>	<b>%Prot</b>
<b>PXD</b>	-363.3	4034.1	34.4
<b>PXT</b>	-297.3	3781.0	32.2
<b>PYD</b>	-270.4	3899.1	33.2
<b>PYT</b>	-323.6	3325.4	28.3
<b>PZD</b>	-345.0	3729.0	31.8

<b>PZT</b>	-277.5	3775.5	32.2
------------	--------	--------	------

It can be pointed out, that the PXD orientation (Fig.S1) is distinctly more probable than the other ones. Besides, this orientation presents a contact surface of the MIP of 4034.1 A<sup>2</sup> which is the largest recorded value for the 6 systems. These MIP contact surface values can also be seen from the PSA protein point of view. Since the protein is free to move during the molecular dynamics simulation, its insertion surface testifies its ability to create favourable interaction with the PPy moieties. Expressed as a percentage of the whole PSA surface, the orientation PXD is again the most promising one, with a value of 34.4% of its surface inserted in the MIP. It can be expected that, when the protein is removed, the MIP would then present a shape useful for the analytical detection of PSA. To sum up, the PXD orientation is the most probable one for the PSA-MIP generation. Therefore, these interactions are described below whereas the reader will find the structural description of the 5 other orientations in the supplementary data of this article (Figures S3 to S7 and tables S1 to S5). The representative structure of MIP/PSA in the PXD orientation is displayed Fig.1. Based on molecular dynamics simulation, it appears that the PSA protein stays deeply inserted in the polymer. The interactions which occur between the PPy and PSA authorize thus the protein to stay inserted in the polymer.

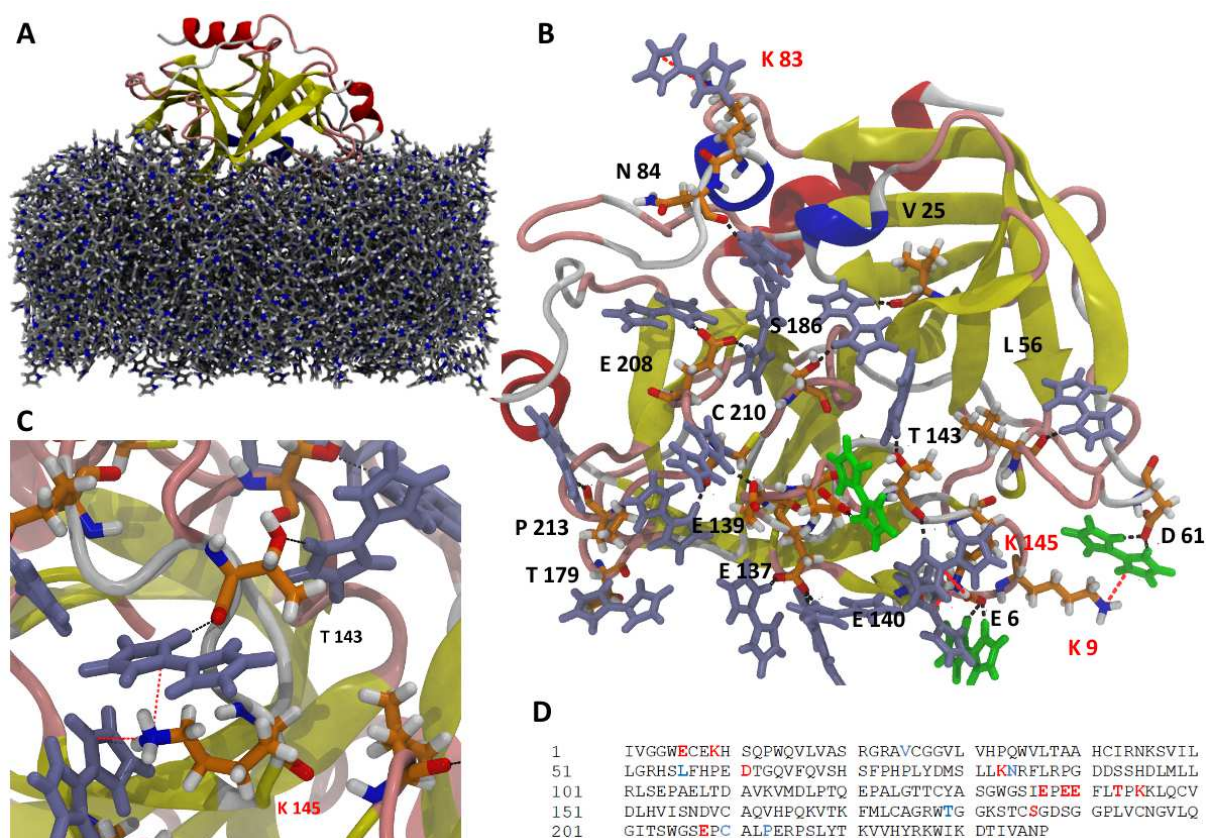


**Fig. 1:** (A) global view of the PSA protein inserted in the MIP polymer along the X down direction. (B) detailed view of the main interactions reported in the table X2 for the X down direction between PSA and MIP polymer. (C) one zoom of one MIP/PSA association (see text). (D) PSA protein sequence where the residues involved in the interactions with PPY are highlighted with red or blue colors for, respectively, sidechain or backbone atoms interactions.

Data presented in Table S6 indicate that the most favourable interactions between PPY and PSA are hydrogen bonds and cation/ $\pi$  interactions. Other dispersive interactions, such as van der Waals (VDW), indubitably exist. However, this effect is not described here since VDW is directly correlated to the contact surface between the two partners. For the PXD orientation, the surface contact is the largest one (table 1) so that this effect is maximal for the PXD orientation.

For all hydrogen bonds presented in table S6, the PPy acts as a donor of hydrogen bonds whereas the PSA is acceptor. Indeed, the aromatic amino moieties of PPy are able to interact with PSA electronegative moieties to form hydrogen bonds. Therefore, there was no doubt that amino-acids such as aspartate (D) or glutamate (E) were the most involved in hydrogen-bond interactions. 21 hydrogen bonds are observed for PSA in the PXD orientation and form a strong network of favorable interactions displayed on Fig.1B. This network involves 18 specific amino-acids of PSA and presented in the sequence of the Fig.1C and in table S6. It can be pointed out that PPy<sub>c</sub> interactions generate two hydrogen bonds toward the carboxylate since, for the cis conformation, both NH vectors of PPy are on the same direction. Therefore, the interactions of PPy<sub>c</sub> with E6, D61 and E140 carboxylate moieties create a total of 6 hydrogen bonds instead of 3. These last ones can be observed on the Fig.1B, with green color for PPy<sub>c</sub>. The positions of the hydrogen bonds in MIP are equally partitioned in deep (D) or border (B) interactions. For the favorable interactions, it can be expected that the presence of B and D types should be crucial for MIP generation. Indeed, MIP must act as a fingerprint of the PSA shape and thus must encompass various locations on the PSA surface. This fact is well illustrated on Fig.1B (or on the sequence of Fig.1D) where the localization of the hydrogen bonds interactions is spread on a large part of the PSA protein

Three cation/ $\pi$  interactions are also observed between PSA and PPy and concern the ammonium cation of some accessible lysine PSA residues (namely K9, K83 and K145) with the aromatic moieties of PPy. These electrostatic interactions are reported on table S6 and displayed with red colors on Fig.1B and 1C. Two of these interactions make one interesting feature: their PPy residues are also implicated with hydrogen bond interactions. This can be easily seen on Fig.1B where K9 makes a cation/ $\pi$  interaction with the PPy<sub>c</sub> residue involved in hydrogen bonds with D61. One other example is presented on Fig.1C where K145 present a similar behavior with a PPy<sub>t</sub> residue hydrogen bonded with T143. These facts demonstrate

that the cation/ $\pi$  interaction, in addition to its favorable association with PSA, can provide a stabilizing role of the hydrogen bond network described above.

These different calculations permitted to comfort the choice of PPy as a polymeric matrix of a molecular imprinted polymer for PSA protein model. Electrochemical measurements were then investigated to optimize MIPs synthesis parameters, and to perform selectivity tests prior to PSA sensing in simple and complex media.

## **3.2. Electrochemical experimental results**

### **3.2.1. Optimization of MIP experimental parameters**

MIP's thickness, duration of templates incubation, nature of the extractor and further elution duration were optimized to guarantee the efficiency and accuracy of the designed PPy MIP based sensor.

The MIP thickness was optimized by square wave voltammetry, using different pulse widths from 3 s to 20 s. Results presented in Fig. S8 indicate that PSA peak intensity reaches a maximum for a pulse width of 7 s. MIPs were thus prepared by CA at a fixed potential of 1.05 V vs. SCE during 7 s.

Incubation time is another important parameter, as it strongly influences the binding capacity between a designed MIP and the analytes of interest. Here, we have immersed a freshly extracted MIP sensor into a  $3 \cdot 10^{-8}$  M PSA solution during 5, 10, 15, 20 and 25 min. Results presented in Fig. S9 indicate that PSA peak current increases versus incubation time and that it reaches a steady state at 20 min. Consequently, the incubation duration was fixed at 20 min.

In the present work, PSA elution was performed by dipping the MIP coated electrodes in a sur-saturated NaCl solution and by subsequent washing with double ionized (DI) water. In fact, high electrolytes concentrations can affect protein physical stability by modifying their conformations and modulating the strength of electrostatic interactions within them. This may

cause proteins folding, which leads to their removal from the PPy polymer (Chi et al., 2003; Dill et al., 1990).

Results gathered in Table S7 show that the maximum extraction percentage was reached after 3 min dipping into the sur-saturated NaCl solution and 30 min rinsing with DI water. This approach was applied for the extraction of PSA templates from the PPy polymeric matrix.

### **3.2.2. Electrochemical characterization of MIPs and NIPs based sensors**

Cyclic voltammetry was investigated to characterize the electrochemical response of the MIP and NIP based sensors before and after immersion in the sur-saturated NaCl solution. The MIP based sensor voltammogram, presented in Fig. S10, displays an oxidation peak at 0.29 V which is related to the presence of PSA protein. The absence of this characteristic peak for the NIP coated electrode and for both MIP and NIP sensors dipped in the extraction solution confirms that: i) the protein template is embedded in the imprinted polymeric network, ii) washing with sur-saturated NaCl / DI water solutions permits to remove PSA from the imprinted polymer, and iii) the absence of specific binding sites for the NIP based sensor.

### **3.2.3. Morphological characterization of MIPs and NIPs surfaces**

Atomic force microscopy (AFM) was used to characterize the morphology of MIP and NIP films. Images, presented in Fig. S11, show that the MIP morphology changes considerably after immersion in a sur-saturated NaCl solution, while that of the NIP remains quasi-unchanged.

To better understand the morphological difference between these films, we have considered three statistical parameters deeply representative of surfaces roughness: the root-mean square height,  $S_q$ , the maximum surface peak height,  $S_p$ , and the maximum surface valley depth,  $S_v$  (Fig. S12 and table S8). Estimated in the spatial frequency range: 0.5 to 512  $\mu\text{m}^{-1}$ ,  $S_q$ ,  $S_p$  and  $S_v$  values of the MIP were of order of 32.6 nm, 93.4 nm and 102.5 nm respectively. These values decrease significantly, after the extraction process, to attain 4.0 nm, 31.6 nm and 15.0 nm respectively. In the case of the NIP,  $S_q$ ,  $S_p$  and  $S_v$  values were found of order of 3.1 nm, 11.4 nm and 26.1 nm, respectively. These

parameters remain quasi constant after its further dipping in a sur-saturated NaCl solution (of order of 2.8 nm, 23.4 nm and 14.9 nm for  $S_q$ ,  $S_p$  and  $S_v$  values respectively). This proves that the extraction procedure has no effect on NIP films whereas it removes efficiently PSA templates from the MIP ones. These results are well correlated to the electrochemical ones (Fig. S10), as the voltammograms of the “extracted” MIP and those of the NIP before and after extractive liquid use, are quite comparable.

### **3.2.4. FTIR characterization of MIP and NIP**

FTIR analysis were performed to characterize PSA binding to PPy via the determination of functional groups involved in the interaction between the template and the polymeric matrix. FTIR spectra of the MIP and the NIP are depicted in Fig. S13. For both spectra we observe the pyrrole ring C-C, C=C stretching vibration ( $1547\text{ cm}^{-1}$ ) (Ahmad et al., 2016) the =C H in plane, C-N stretch and =C H out of plane vibration at  $1454$ ,  $1307$  and  $910\text{ cm}^{-1}$  respectively (Zhang et al.; 2013, Ruhi et al., 2014, Cordeiro et al., 2015). The band at  $1190\text{ cm}^{-1}$  is ascribed to =C-H out of plane vibration band, that at  $1035\text{ cm}^{-1}$  corresponds to N-H in plane deformation. The band at  $690\text{ cm}^{-1}$  is relative to =C-H out of plane vibration (Ruhi et al., 2014). The great similarity between these two spectra is related to the fact that MIP and NIP have the same polymeric backbone.

The presence of amine ( $1620\text{ cm}^{-1}$ ), amide ( $1680\text{ cm}^{-1}$ ), out-of-plane NH ( $804\text{ cm}^{-1}$ ) and S-S stretch ( $550\text{ cm}^{-1}$ ) bands, appearing only in the FTIR spectrum of the MIP, arise from PSA protein which is embedded in the polymeric matrix of the MIP.

### **3.2.5. Sensors analytical performances**

Square wave voltammetry was investigated to follow up the response of the MIP-based sensor towards increasing PSA concentrations, ranging from  $3 \times 10^{-8}\text{ ng/ml}$  to  $300\text{ ng/ml}$ . Voltammograms presented in Fig.S14, indicate that the current peak value, which corresponds to PSA oxidation potential, is concentration dependent.

The same experiments were conducted with NIP-based sensors. A quasi constant peak current was recorded for the whole PSA concentration range. Besides, this value is lower than that obtained with a MIP incubated in a  $3 \times 10^{-8}$  ng/ml PSA solution. This means that nonspecific adsorption is negligible and doesn't account for MIP responses, even for low PSA concentrations.

### 3.2.6. Sensors selectivity tests

Before potential use of the MIP-based sensor as reliable tool for PSA quantification, we investigated its response in presence of three proteins: bovine serum albumin (BSA), immunoglobulin G (IgG) and immunoglobulin M (IgM). Three MIP based sensors were thus prepared, extracted, and incubated separately, during 20 min, in  $10^{-8}$  M of each analyte of interest. Results (Fig. S15) indicate that the current response of the sensor toward PSA was about one order of magnitude higher than that of BSA, IgG and IgM. Moreover, electrochemical responses of these three interferents were of the same order of magnitude as that obtained by incubating a NIP based sensor in a PSA solution. Hence, the realized MIP-based sensor is selective enough, to consider its output current as pertinent parameter to quantify PSA concentration in any media.

### 3.2.7. Calibration curve for further PSA quantification

SWV current peak variations versus PSA concentrations are reported on Fig. 2. Among the large variety of biochemical models, Hill equation (eq.1) was found to be the most accurate one to fit experimental data

$$I(C) = \frac{A \times C^\alpha}{K_d^\alpha + C^\alpha} \quad (\text{eq. 1})$$

$I(C)$  corresponds to the current variations for a given PSA concentration ( $C$ );  $K$  is the equilibrium dissociation constant,  $A$  is an empiric constant, and  $\alpha$  is the Hill coefficient.

The equilibrium dissociation constant  $K_d$ , that accounts for the strength of the binding between PSA and its imprint in the PPy film, was estimated at  $K_d = (1.02 \pm 0.54) \times 10^{-14}$  M. This value, largely lower than those presented in other studies concerning protein detection with a MIP, confirm computational calculations findings which state the existence of numerous favourable interactions between PPy and PSA.

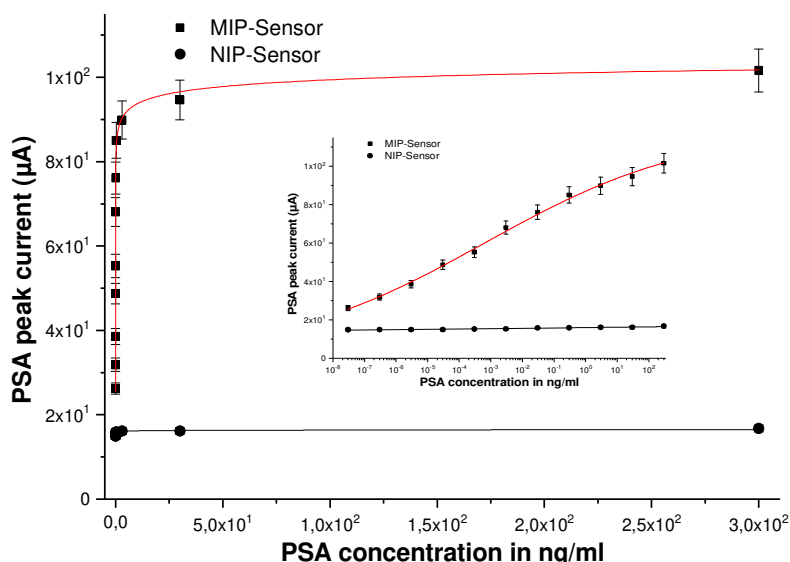


**Fig. 2:** Current variations of MIP-PSA and NIP-PSA based sensors, versus PSA concentration. Inset: Calibration curves of MIP-PSA and NIP-PSA in logarithmic scale.

Indeed, calculations emphasizes the adaptability of PPy polymer toward PSA and demonstrate that the cation/ $\pi$  interaction afford a stabilizing role of the hydrogen bond network.

The fact that the experimental values can be accurately fitted by a given function, rends possible the quantification of a PSA concentration in complex media such as unidentified human serums.

### 3.2.8. PSA quantification in human serums

Serum samples of thirty-five patients have been considered to assess the reliability of the MIP-based sensor. Blind tests were conducted to determine the PSA concentration of each

sample, according to the calibration curve of the sensor (Fig.3). Then, estimated values were compared to those obtained by the standard enzyme-linked immunosorbent assay (ELISA).

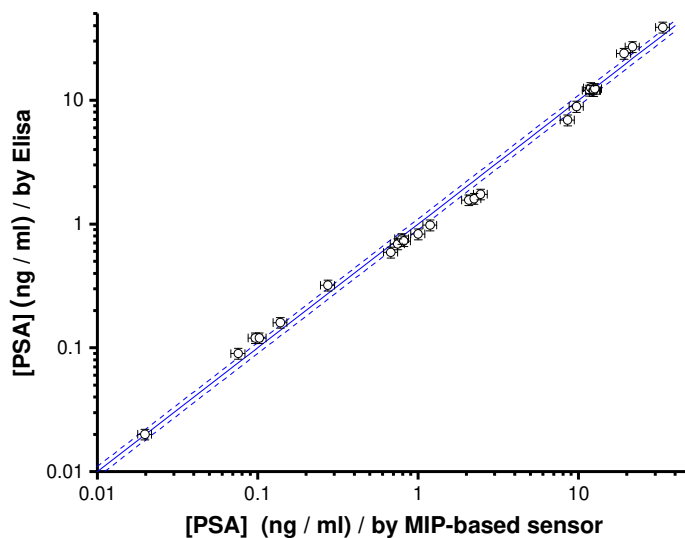


**Fig.3.** Comparison of the PSA concentrations in patient serum samples determined with the MIP based sensor and the ELISA method.

As shown in Fig.3, PSA concentrations estimated by the two methods are quasi-identical, a straight line is obtained with a slope close to the unity:  $0.990 \pm 0.017$ . These very encouraging results pave the way for a new reliable method that uses molecular imprinted polymers as artificial receptors. The robustness, reliability and relative ease of use, make such biomimetic sensors suitable for precocious diagnosis of several pathologies like cancers and of Alzheimer disease.

#### 4. Conclusion

In this study, the interactions between a protein model amino-acids and polymer residues were defined and evaluated using a molecular dynamics (MD) study. Prostate-specific antigen (PSA) and polypyrrol-based polymeric matrix (PPy) were selected for the interest in

the diagnosis of prostate cancer and the ability to host PSA molecules, respectively. Calculations indicate that whatever are the starting orientations of the PSA/PPy system, all PSA molecules remain inserted in the PPy polymer, suggesting a strong binding between the designed MIP and the PSA protein. This can explain why PPy is often chosen as MIPs' polymeric matrix. The most probable orientation, PXD, allowed PSA/MIP interactions with the lowest adsorption energy and the highest contact area between proteins and the MIP.

Accordingly, a PPy MIP based electrochemical sensor was designed and optimized (electropolymerization conditions, duration of protein incubation, the nature of the extractor and further elution duration...) to fulfil the analytical field exigencies. The designed electrochemical sensor exhibited a low limit of detection, a high selectivity, good reproducibility and fast rebinding capacity. Besides, it requires a simple implementation and low manufacturing costs, in comparison to classical biosensors that use antibodies or enzymes for examples.

The proposed sensor was successfully applied for the determination of PSA concentration in human serum samples without any cross-reactivity and the obtained result agreed well with those obtained by the standard ELISA method.

In fine, the developed MIP-based-biosensor can be considered as an attractive candidate for trace level protein detection and supply valuable information for early clinical diagnostics.

### **Conflicts of interest**

The authors report no conflicts of interest in this work.

### **Acknowledgements**

This work benefited from the access to the supercomputing facilities of the GENCI (Grand Equipement National pour le Calcul Informatique). ANR (Agence Nationale de la Recherche)

and CGI (Commissariat à l'Investissement d'Avenir) are gratefully acknowledged for their financial support of this work through Labex SEAM (Science and Engineering for Advanced Materials and devices) ANR 11 LABX 086, ANR 11 IDEX 05 02.

A part of this work was funded by Campus France and CMCU committee via the project PHC Utique 16G0808.

## References

Ahmad, Z., Choudhary, M. A., Mehmood, A., Wakeel, R., Akhtar, T., Rafiq, M. A., 2016. *Macromol. Res.*, 24, 596-601.

Akter, R., Jeong, B., Rahman, Md. A., 2015. *Analyst.* 140, 995-998.

Bel Bruno, J. J., 2019. *Chem. Rev.* 119, 94-119.

Boroznjak, R., Reut, J., Tretjakov, A., Lomaka, A., Öpik, A., Syritski, V., 2017. *J. Mol. Recognit.* 1-9.

Case, D.A., Ben-Shalom, I.Y., Brozell, S.R., Cerutti, D.S., Cheatham, T.E., Cruzeiro V.W.D., Darden T.A., Duke, R.E., Ghoreishi, D., Gilson, M.K., Gohlke, H., Goetz, A.W., Greene, D., Harris, R., Homeyer, N., Izadi, S., Kovalenko, A., Kurtzman, T., Lee, T.S., LeGrand, S., Li, P., Lin, C., Liu, J., Luchko, T., Luo, R., Mermelstein, D.J., Merz, K.M., Miao, Y., Monard, G., Nguyen, C., Nguyen, H., Omelyan, I., Onufriev, A., Pan, F., Qi, R., Roe, D.R., Roitberg, A., Sagui, C., Schott-Verdugo, S., Shen, J., Simmerling, C.L., Smith, J., Salomon-Ferrer, R., Swails, J., Walker, R.C., Wang, J., Wei, H., Wolf, R.M., Wu, X., Xiao, L., York, D.M., Kollman, P.A., 2018. *AMBER 2018*, University of California, San Francisco.

CA, T., CC, Y., YW, L., VAL, R., 2018. *J control release.* 287, 24-34

Chianella, I., Karim, K., Piletska, E. V., Preston, C., Piletsky, S. A., 2006. *Anal. Chim. Acta.* , 73-78

Chianella, I., Lotierzo, M., Piletsky, S. A., Tothill, I. E., Chen, B., Karim, K., A. Turner, P. F., 2002. *Anal. Chem.* 74, 1288-1293.

Chi, E.Y., Krishnan, S., Randolph, T.W., Carpenter, J. F., 2003. *Pharmaceutical research.* 20, 1325-1336.

Cordeiro, E. R., A. Fernandes, W. C., Pereira, A. F. C., da Costa, M. M., Nascimento, M. L. F., de Oliveira, H. P., 2015. *Quim. Nova*, 38, 1075-1079.

Dabrowski, M., Cieplak, M., Sindhu Sharma, P., Borowicz, P., Noworyta, K., Lisowski, W., D'Souza, F., Kuhn, A., Kutne, W., 2017. *Biosens; Bioelectron.* 94,155-161.

Dabrowski, M.,Lach, P.,Cieplak, M., Kutner, W., 2018. *Biosens. Bioelectron.* 102, 17–26.

Darden, T., York, D., Pedersen, L., 1993.*J. Chem. Phys.* 98, 10089-10092.

De, M., Rana, S., Akpınar, H., Miranda, O. R., Arvizo, R. R., Bunz, U.F., Rotello, V.M., 2009. *Nat. Chemistry.* 1, 461-465.

Dill, K.A., 1990. *Biochemistry.* 29, 7133-7155

Ebarvia, B. S., Cabanilla, S., Sevilla, F., 2005. *Talanta.* 66, 145-152.

El-Sharif, H. F., Stevenson, D., M.Reddy, S., 2017. *Sens. Actuator B-Chem.* 241, 33–39.

Erdossy, J., Horváth, V., Yarman, A., Scheller, F. W., Gyurcsányi, R., 2016. *Trends Anal. Chem.* 79, 179–190.

Ertürk, G., Hedstrom, M., Tümer, M. A., Denizli, A., Mattiasson, B., 2015. *Analy. Chim. Acta.* 891, 120-129.

Farooq, S., Nie, J., Cheng, Y., Yan, Z., Li, J., Bacha, S. A. S., Mushtaq, A., Zhang, H., 2018. *Analyst.* 143, 3971-3989.

Fu,J., Chen, L., Li, J., Zhang, Z., 2015. *J. Mater. Chem. A.* 3, 13598-13627

Frasco, M. F., Truta, L. A. A. N. A., Sales M. G.F., Moreira F. T. C., 2017. *Sensors.* 17, E523

Heredia, A., Latinovic, Barbault, O. S., F., de Leeuw, E. P., 2015. *Drug Des. Dev. Ther.* 9, 5469-5478.

Humphrey, W., Dalke, A., Schulten, K., 1996. *J. Mol. Graph.* 14,33-38.

Hwang, D. G.,Chae, Y. M., Choi, N., Cho, I.J., Kang, J. Y., Lee, S. H., 2017. *Microsyst Technol.* 23, 1207–1214.

Jolly, P., Tamboli, V., Harniman, R. L., Estrela, P., Allender, C. J., Bowen, J. L., 2016. *Biosens. Bioelectron.* 75, 188–195

Jonquoy, A.,Mugniery, E., Benoist-Lasselin, C., Kaci, N.,Le Corre,L., Barbault, F., Girard, A.-L., Le Merrer, Y.,Busca, P.,Schibler, L.,Munnich, A.,Legeai-Mallet, L., 2011. *Hum mol genet.* 21, 841–851.

Khan, M. S., Dighe, K., Wang, Z., Srivastava, I., Daza, E., 2018. *Analyst.*143, 1094.

Ktari, N., Fourati, N., Zerrouki, C., Ruan, M., Seydou, M. , Barbaut, F., Nal, F.,Yaakoubi, N., Chehimi, M. M.,Kalfat, R., 2015. *RSC Advances.* 5, 88666 -88674.

Lai, Y., Deng, Y., Yang, G., Li, S., Zhang, C., Liu, X., 2018. *J. Biomed. Nanotechnol.* 14, 1688-1694.

Lorenzo, R. A., Carro, A. M., Alvarez-Lorenzo, C., Concheiro, 2011. *Int. J. Mol. Sci.* 12(7), 4327–4347.

Maier, J. A., Martinez, C., Kasavajhala, K., Wickstrom, L., Hauser, K. E., Simmerling, C., 2015. *J. Chem. Theory Comput.* 11, 3696-3713.

Martínez, L., Andrade, R., Birgin, E. G., Martínez, J. M., 2009. *J Comput Chem.* 30, 2157-2164.

Ma, Y., Shen, X. L., Zeng, Q., Wang, L.S., 2017. *Microchim. Acta.* 148, 4469-4476.

Mazouz, Z., Rahali, S., Fourati, N., Zerrouki, C., Aloui, N., Seydou, M., Yaakoubi, N., Chehimi, M.M., Othmane, A., Kalfat, R., 2017. *Sensors.* 17, 2586.

Ménez, R., Michel, S., Muller, B. H., Bossus, M., Ducancel, F., Jolivet-Reynaud, C., Stura, E. A., 2008. *J. Mol. Biol.*, 376, 1021-1033.

Mohsenzadeh, M.S., Mohammadinejad, A., Mohajeri, S. A., 2018. *Food Addit Contam: Part A.* 1-16.

Monti, S., Cappelli, C., Bronco, S., Giusti, P., Ciardelli, G., 2006. *Biosens. Bioelectron.* 22, 153-163.

Ogasawara, Y., Shida, Y., Takikawa, M., Funaki, Y., Suzuki, T., Koike, S., 2015. *J. Chromatography B.* 997, 136-141.

Ozcan, L., Sahin, Y., 2007. *Sens Actuators B.* 127, 362-369.

Özcan, L., Şahin, M., Şahin, Y., 2008. *Sensors.* 8, 5792–5805.

Patra, S., Roy, E., Madhuri, R., Sharma, K. P., 2015. *Biosens. Bioelectron.* 66, 1–10.

Rodríguez-Dorado, R., Carro, A. M., Chianella, I., Karim, K., Concheiro, A., Lorenzo, R. A., Piletsky, S., Alvarez-Lorenzo, C., 2016. *Anal. Bioanal. Chem.* 408, 6845-6856.

Ramanaviciene, A., Ramanavicius A., 2004. *Biosens Bioelectron.* 20, 1076–1082.

Roe, D. R., Cheatham, T. E., 2013. *J. Chem. Theory Comput.* 9, 3084-3095.

Rao, H., Lu, Z., Ge, H., Liu, X., Chen, B., Zou, P., Wang, X., He, H., Zeng, X., Wang, Y., 2017. *Microchim. Acta.* 184, 261-269.

Rebello, S.C.R., Santosd, C., Costa-Rodriguesc, J., Fernandesc, M.H., Noronha, J. P., Goreti, M., Sales, F., 2014. *Electrochim. Acta.* 132, 142–150.

Ruan, M., Seydou, M., Noel, V., Piro, B., Maurel, F., Barbault, F., 2017. *Phys. Chem B.* 121, 4071–4080.

Ruhi, G., Bhandari, H., Dhawan, S. K., 2014. *Prog Org Coat*, 77, 1484-1498.

Ryckaert, J. P., Ciccotti, G., Berendsen, H. J. C., 1977. *J. Comput. Phys.* 23, 327–41.

Scorrano, S., Mergola, L., Del Sole, R., Vasapollo, G., 2011. *Int. 6J. Mol. Science.* 12, 1735–1743.

Si, B., Song, E., 2018. *Chemosensors.* 6, 1.

Sindhu, S. P., Wojnarowicz, A., Sosnowska, M., Benincori, T., Noworyta, K., D'Souza, F., Kutner, W., 2016. *Biosens. Bioelectron.* 77, 565–572.

Spivak,D.A., Shea, K. J., 1998. *Macromolecules.* 31, 2160-2165

Stura, E. A., Muller, B. H., Bossus, M., Michel, S., Jolivet-Reynaud, C., Ducancel, F., 2011. *J. Mol. Biol.* 414, 530-544.

Touzeau, J., Barbault, F., Maurel, F., Seydou, M., 2018. *Chem. Phys. Lett.*, 713, 172-179.

Vasilescu, A., Gaspar, S., Mihai, I.,Tacheb, A., Litescu, S. C., 2013. *Analyst.* 138, 3530- 3537.

Wilson, A. J., 2009. *Nat. Chemistry.* 1, 429-430.

Xiao, D., Jiang, Y., Bi, Y., 2018.*Microchim. Acta.* 185 – 247.

Yazdani, Z., Yadegari, H., Heli, H., 2018.*Anal. Biochem.* 566, 116-125.

Zeng, Q., Huang, X., Ma, M., 2017. *Int. J. Electrochem. Sci.b.* 12, 3965–3981.

Zhang, B., Gao, W., Piao, J., Xiao, Y., Wang, B., Peng, W., Gongga, X., Wang, Z., Yang, H., Chang, J., 2018. *ACS Appl. Mater. Interfaces.*, 10, 14549–14558.

Zhang, Y., Zhang, Z., Xu, S., Yu, L., Tang, Q., 2013. *RSC Adv*, 1-9.

Zhao, C., Ma, X., Li, J., 2017. *Chin J Anal Chem.* 45, 1360-1366.

## **Web references**

WEB1: RCSB Protein Data Bank - RCSB PDB, <https://www.rcsb.org/pdb/home/home.do>,  
(accessed December 13, 2017).